Improved Atmospheric Solar Radiation Budget Pyranometry

GOTTFRIED HÄNEL AND KARIN KASTNER

Institute of Meteorology and Geophysics, Johann Wolfgang Goethe University, Frankfurt am Main, Germany

(Manuscript received 21 April 1999, in final form 24 August 1999)

ABSTRACT

The solar radiation budget is investigated with seven pyranometers. Three of these instruments have horizontally aligned sensors. The sensors of the remaining four instruments are vertically aligned in such a way that their normals point to the north, south, east, and west. With this system, the authors are able to detect all properties of interest for radiation budget considerations. These are the flux densities of direct solar, diffuse-sky, global, and reflected radiation; the vector of the solar net flux density; and the solar radiation supply (for atmospheric absorption and/or photochemical processes). Equations for the vector of the net flux density and the radiation supply in terms of the pyranometer readings are derived and discussed.

Whenever the solar radiation supply and the mean solar absorption coefficient of the atmosphere or of specific atmospheric species are known, the relevant solar volume absorption rate and the appertaining solar heating rate of the atmosphere can be calculated without any assumptions. This method is applicable during any weather situation throughout the entire atmosphere.

Simple parameterizations of the radiation supply and the total atmospheric heating during the daylight period due to absorption of solar radiation by particles are discussed.

1. Introduction

Pyranometry is a common tool for the study of the solar radiation budgets of the earth's surface (e.g., Ambach 1963) and the atmosphere (e.g., Roach 1961; Murai et al. 1976; Valero et al. 1982). For these purposes, instruments with horizontally aligned sensors are used to detect the global and the reflected solar radiation at the surface and at different heights in the atmosphere.

Such measurements taken at the surface immediately yield the solar radiation absorbed by the ground. The absorption of solar radiation in an atmospheric layer is obtained by taking such measurements at its upper and lower boundaries and approximating the divergence of the net flux density vector of solar radiation by the contribution coming from its vertical component alone (simplified divergence method). This kind of data evaluation is believed to give reliable results for a cloudless, horizontally homogeneous atmosphere above a homogeneous earth surface around local noon (e.g., Roach 1961; Valero et al. 1982; and section 5b of this paper). Horizontally homogeneous cloud layers can also be studied in this way.

A rigorous divergence determination requires the simultaneous measurement of the net flux density vector at four space points using a total of 24 pyranometers (see section 2b and Fig. 1). The implementation of this method requires an extreme effort so that its realization in the atmosphere seems to be unlikely.

Because of the restrictions of the simplified divergence method mentioned above, experimentally based data of absorption of solar radiation in the atmosphere are rare. It is also a deficiency that the method yields the absorption by all absorbing species together but not the contributions from specific absorbing species separately. In order to obtain information of this kind, the total absorption has to be interpreted using additional assumptions and approximations. In this situation, Hänel et al. (1982) developed new ideas to determine in situ the time rate of solar energy transformed into internal energy due to absorption by specific atmospheric species. The new method is applicable during all kinds of atmospheric conditions. It involves the determination of the absorption coefficients of the atmospheric species taken into consideration and of the solar radiation supply. Results of the absorption by particles and water vapor have been given already by Busen and Hänel (1987) and Hänel et al. (1990).

One of the main problems of the new absorption determination technique was the measurement of the solar radiation supply. For this, specific instruments had been constructed, but the maximum possible error involved was on the order of 10%–20%. In this paper, we present a considerably improved determination of the radiation supply based on measurements with a specific arrange-

Corresponding author address: Dr. Gottfried Hänel, Johann Wolfgang Goethe University, Georg Voigt Strasse 14, D-60325 Frankfurt am Main, Germany.
E-mail: hanel@meteor.uni-frankfurt.de

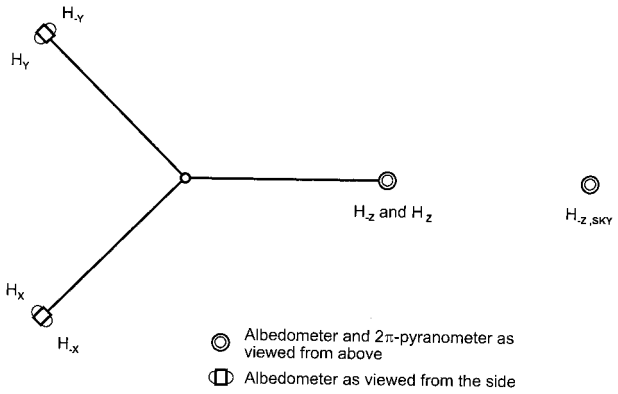

FIG. 1. Schematic illustration of the orientation of sensors and their arrangement for radiation budget pyranometry as viewed from above.

ment of seven commercially available pyranometers for the detection of solar radiation. The maximum possible error with the new method is on the order of 3%–6%.

In addition, the new arrangement of pyranometers also yields the vector of the net flux density of solar radiation in situ and without any assumptions. This enables us to discuss on an experimental basis the restrictions of the simplified flux divergence method mentioned above.

Currently, absorption data for cloudy atmospheres, especially situations with strong but incomplete cloud cover, are rare. This is a major deficiency regarding the need for long-term weather forecast and climate modeling. Consequently, we present and discuss results of the influence of cloudiness on the solar radiation supply, the vector of the solar net flux density, and the absorption of solar radiation by particles.

2. Theory

In this section, we compile all basic equations to be used in the subsequent text. These are the energy budget equation for solar radiation, the equations of the heating rate of the atmosphere due to absorption of solar radiation, the vector of solar net flux density, and the solar radiation supply, the latter two being functions of the pyranometer readings.

a. Energy budget equation for solar radiation and atmospheric heating rate

The equation of radiative transfer describing the change of the spectral radiance along the path of radiation through the atmosphere is the starting point for all further considerations, and reads

$$\frac{dN_\lambda}{ds} = -\sigma_{E\lambda}N_\lambda + \sigma_{E\lambda}Q_\lambda, \tag{1}$$

where N_λ is the spectral radiance, ds is the distance element along the path of radiation (beam), $\sigma_{E\lambda}$ is the volume extinction coefficient of the atmosphere at the wavelength λ, and Q_λ is the spectral source function (spectral source radiance). The first term on the right side describes the attenuation of radiation due to absorption and scattering, and the second term describes the intensification of radiation due to scattering into the beam and emission. Integration of Eq. (1) over all beam directions and over the entire spectrum of solar radiation yields the energy budget equation of solar radiation, which can be written in the form

$$\overline{\frac{1}{c_\lambda}}\frac{\partial S}{\partial t} + \nabla \cdot \mathbf{F}_N = -\overline{\sigma}_{\mathrm{AS}}S + \overline{\sigma}_{\mathrm{AB}}B, \tag{2}$$

where

$$S = \int_{0.3\,\mu\mathrm{m}}^{3.5\,\mu\mathrm{m}} \int_{4\pi\mathrm{sr}} N_\lambda \, d\Omega \, d\lambda$$

$$= \text{solar radiation supply} \tag{3}$$

$$\mathbf{F}_N = \int_{0.3\,\mu\mathrm{m}}^{3.5\,\mu\mathrm{m}} \int_{4\pi\mathrm{sr}} \mathbf{N}_\lambda \, d\Omega \, d\lambda$$

$$= \text{vector of solar net radiation flux density}, \tag{4}$$

where t is time; λ is the wavelength of radiation; Ω is the solid angle; B is the integral of the spectral radiance B_λ of the blackbody radiation over all directions and over the entire solar spectrum from wavelengths 0.3 to 3.5 μm; $\mathbf{N}_\lambda$ is the spectral radiance vector; and $\overline{1/c_\lambda}$, $\overline{\sigma}_{\mathrm{AS}}$, $\overline{\sigma}_{\mathrm{AB}}$ are the weighted integral mean values over all directions and over the entire solar spectrum from wavelengths 0.3 to 3.5 μm of the reciprocal of the velocity of light and of the absorption coefficient of the atmosphere, with $\partial N_\lambda/\partial t$, N_λ, and B_λ as weights, respectively. For a discussion of the solar radiation supply and the vector of solar net radiation flux density, see section 2b.

On the left side of the solar energy budget Eq. (2), the first term is the local change of the energy density of the solar radiation with time, and the second term is the local influx–outflux balance of the solar radiation of a volume element. Normally, the first term is negligible compared with the second term. On the right side, the first term is the negative volume absorption rate—that is, the sink of the solar radiation due to absorption—and the second term is the volume emission rate—that is, the source due to emission. Considering the entire solar spectral region, emission is negligible compared with absorption. Thus, we obtain as an excellent approximation

$$\nabla \cdot \mathbf{F}_N \cong -\overline{\sigma}_{\mathrm{AS}}S. \tag{5}$$

For a cloudless, horizontally homogeneous atmosphere over a homogeneous earth surface at local noon, it is assumed that the approximation

$$\nabla \cdot \mathbf{F}_N \approx \partial F_{\mathrm{NZ}}/\partial \mathbf{z} \tag{6}$$

is valid, where F_{NZ} is the vertical component of $\mathbf{F}_N$. Consequently, investigators tried to obtain the absorp-

tion of the solar radiation by all absorbing species of the atmosphere by measuring F_{NZ} as a function of z. For this measurement, normally two pyranometers detecting solar radiation are aligned horizontally so that their sensor surfaces point upward and downward. Determination of absorption using the right side of Eq. (6) involves the measurement of small differences of large quantities. Thus, no in situ measurement of absorption can be carried out with this simplified divergence method. Only more or less extended atmospheric layers can be studied. For this, the atmosphere has to be (practically) cloudless (e.g., Valero et al. 1982), or a horizontally homogeneous cloud layer might be present.

In contrast, the absorption of solar radiation can be determined everywhere in the atmosphere in situ and without any assumptions by measuring the properties of the volume absorption rate $\overline{\sigma}_{AS}S$ on the right side of Eq. (2). Moreover, since the weighted mean absorption coefficient of the atmosphere $\overline{\sigma}_{AS}$ is the sum of the weighted mean absorption coefficients of all absorbing atmospheric species, the contributions by specific species may be determined separately. The disadvantage of the in situ method is that there are at least two properties to be known and that the determination of the solar radiation supply and of the absorption coefficients of specific species are more complicated than the measurement of F_{NZ} [see Busen and Hänel (1987) and Hänel (1987, 1994)].

Up to now, the in situ method has been in the development stage [Hänel (1994) and this paper] and therefore has been applied only to the atmosphere near the ground. In contrast, the simplified divergence method has been used repeatedly from flying platforms for studies of the energy budget (e.g., Roach 1961; Murai et al. 1976; Valero et al. 1982).

Finally, the heating rate of the atmosphere due to absorption of solar radiation must be mentioned. It reads

$$\left(\frac{dT}{dt}\right)_S = \frac{1}{\rho c_p}\overline{\sigma}_{AS}S, \tag{7}$$

where ρ is the density and c_p is the specific heat at constant pressure of the air. Equation (7) yields a maximum possible atmospheric heating rate, assuming that no absorbed solar energy is used for other purposes: for example, photochemical reactions. As indicated above, this heating rate can be split easily into the contributions of single absorbing species. The most important absorbers within the entire solar spectral region are particles and water vapor.

b. Vector of net flux density and radiation supply

In this subsection we present the formulas for the vector of net flux density and the radiation supply in terms of the pyranometer readings. According to Eqs. (3) and (4), both properties are integrals over all directions. In regard to the vector of net flux density, the integral of the radiance vector is taken, whereas in regard to the radiation supply, the integrand is the radiance itself—that is, the length of the radiance vector. Thus, contributions to these integrals from opposite directions cancel each other out partly or completely in terms of the vector of net flux density, but they are summed taking the radiation supply into account. Consequently, an arrangement of pyranometers giving exact results for one of these properties cannot yield the same for the other property. With our arrangement to be described below, we obtain the vector of net flux density exactly and obtain an approximation to the radiation supply.

TABLE 1. Notations and descriptions of the pyranometer readings.

Symbol	Direction of radiation	Name
H_X	West to east	The horizontal component of net radiation in the positive x direction
H_{-X}	East to west	The horizontal component of net radiation in the negative x direction
H_Y	South to north	The horizontal component of net radiation in the positive y direction
H_{-Y}	North to south	The horizontal component of net radiation in the negative y direction
H_Z	Upward	The vertical component of net radiation in the positive z direction, reflected radiation
H_{-Z}	Downward	The vertical component of net radiation in the negative z direction, global radiation
$H_{-Z,\,SKY}$	Downward	Sky radiation
$H_{-Z,\,DIR} = H_{-Z} - H_{-Z,\,SKY}$	Downward	Direct solar radiation

1) DESCRIPTION OF MEASURED IRRADIANCES

For our measurements, we use seven standard pyranometers, each of them detecting the solar radiation from a hemisphere (2πsr solid angle)—that is, regarding all possible directions of rays from a hemisphere. Each detector measures an irradiance, more specifically a hemispherical integral of the vertical component of the radiance with respect to the sensor surface. Figure 1 shows schematically the arrangement of pyranometers as they are used during the measurements. The notations and descriptions of the pyranometer readings are compiled in Table 1.

2) VECTOR OF SOLAR NET FLUX DENSITY

We denote **x**, **y**, and **z** to be the unit vectors in the positive x, y, and z directions of a Cartesian coordinate system. The x, y, and z axes point eastward, northward, and upward, respectively. Then, regarding the meaning

of the irradiances according to Table 1, the vector of solar net flux density reads

$$\begin{aligned}\mathbf{F}_N &= F_{\mathrm{NX}}\mathbf{x} + F_{\mathrm{NY}}\mathbf{y} + F_{\mathrm{NZ}}\mathbf{z}\\ &= (H_X - H_{-X})\mathbf{x} + (H_Y - H_{-Y})\mathbf{y}\\ &\quad + (H_Z - H_{-Z})\mathbf{z},\end{aligned} \tag{8}$$

where H_i represents the irradiance into the direction i; and F_{NX}, F_{NY}, and F_{NZ} are the components of $\mathbf{F}_N$ in our Cartesian coordinate system.

3) Solar radiation supply

According to its definition [(3)], the radiation supply is a flux density representing the integrated radiation flowing from all directions through an infinitesimal atmospheric volume. Ideally, it should be determined by pointing a radiance meter to all directions and integrating the results. With the six pyranometers yielding the irradiances H_X, H_{-X}, H_Y, H_{-Y}, H_Z, and H_{-Z}, we obtain the radiation from all directions. But, in general, with a few directions excluded, we detect radiation from one direction with three sensors at the same time. By summing the six pyranometer readings, we obtain an integral of amplified radiances. The amplification factor depends on the direction of radiation and ranges between 1 and $\sqrt{3}$. Thus, we cannot measure the radiation supply exactly with our arrangement of pyranometers, but we are able to derive a simple but realistic model for it.

Defining

$$H = H_X + H_{-X} + H_Y + H_{-Y} + H_Z + H_{-Z} \tag{9}$$

to be the total solar irradiance, the contribution from a solid angle element $d\Omega$ to H is

$$dH = N\, d\Omega \mathrm{AF} = dS\mathrm{AF}, \tag{10}$$

where

$$N = \int_{0.3\,\mu\mathrm{m}}^{3.5\,\mu\mathrm{m}} N_\lambda\, d\lambda \tag{11}$$

is the solar radiance and

$$\mathrm{AF} = |\cos\theta| + \sqrt{1 - \cos^2\theta}(|\sin\phi| + |\cos\phi|) \tag{12}$$

is the amplification factor. In (12), θ is the zenith angle, and ϕ is the azimuth angle of the direction of radiation (θ is the angle between the positive z axis and the direction of radiation, and ϕ is the angle between the negative y axis and the direction of radiation in the x–y plane, measured counterclockwise).

According to Eq. (10), there is a proportionality between the differentials dH and dS. But the amplification factor and the solar radiance are functions of the direction of radiation. The latter can be observed readily by looking at different regions of the sky. Consequently, we cannot have a direct proportionality between H and S. However, splitting the solar radiation supply into its contributions from the direct solar radiation and the diffuse solar radiation and applying an approximation to the latter only, we can find a linear relationship of the form

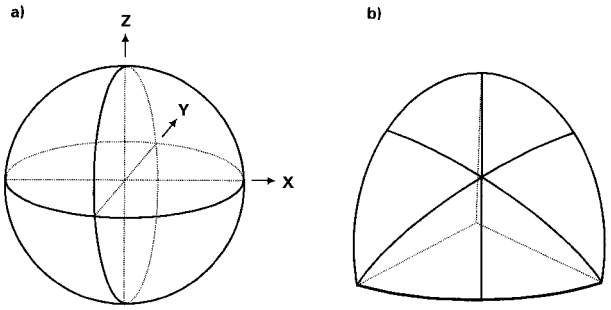

FIG. 2. Schematic illustration of the partition of the entire solid angle (4πsr) into 48 parts. (a) First partition into eight subareas of equal solid angle and shape. (b) Second partition of each of these subareas into six parts of equal solid angle. The first partition yields spherical triangles with equal sides. These triangles are partitioned further by drawing the bisectors of all angles. The resulting spherical triangles are all rectangular and of the same solid angle area. Their corresponding sides are all of the same lengths but are arranged differently.

$$S = c_H H + c_S F_S. \tag{13}$$

Therein, c_H is a constant, c_S is a function of c_H and of the direction of the direct solar radiation, and

$$F_S = (H_{-Z} - H_{-Z,\mathrm{SKY}})/|\cos\theta_S| \tag{14}$$

is the flux density of the direct solar radiation, as measured with a sensor surface normal to the direction of propagation. In (14), θ_S is the zenith angle of the direction of direct solar radiation.

The direct solar radiation has to be considered exactly, since it may determine the order of magnitude of the radiation supply (see Busen and Hänel 1987). The diffuse solar radiation from the sky and from below is treated approximately by dividing the total solid angle area of 4πsr into 48 parts, as shown in Fig. 2. Second, it is assumed that in each of these subareas the radiance can take any value but is isotropic. In this case, all subareas have the same amplification factor $\mathrm{AF}_{\mathrm{SUB}} = 3/2$. Then, by a straightforward calculation, we obtain,

$$c_H = \frac{2}{3}, \qquad c_S = 1 - c_H \mathrm{AF}_S,$$

$$\mathrm{AF}_S = |\cos\theta_S| + \sqrt{1 - \cos^2\theta_S}(|\sin\phi_S| + |\cos\phi_S|), \tag{15}$$

where AF_S is the amplification factor of direct solar radiation and ϕ_s is the azimuth angle of its direction.

The model equations (13)–(15) are exact regarding the direct solar radiation. In case of sky radiation and reflected radiation, any brightness differences among the 48 solid angle subareas are allowed and would be treated exactly if within each of these areas the radiance were isotropic. Consequently, the model error stems only from nonisotropy effects on the level of the individual

subareas. Thus, our subdivision of the total solid angle 4πsr into 48 parts should lead to a good approximation of the sometimes highly variable radiance distributions caused by cloudy skies and coming from patchworklike surfaces with highly different albedos of the elements. It also takes into account shadow effects from nearby buildings or vegetation, as well as bright zones due to reflected radiation from nearby walls.

In contrast to the situations mentioned above, it is possible to estimate the model error for clear-sky conditions and an isotropically reflecting surface. To obtain maximum errors, we simulated extreme clear-sky conditions with a maximum possible variation of the sky radiance: 1) The sky radiance was calculated according to the single scattering approximation, thus neglecting the damping of the sky radiance variation by multiple scattering. 2) We took the highly anisotropic phase function of scattering by particles and thus neglected the damping contribution from the air molecules. From the results, the exact values of the radiation supply and of all irradiances occurring in the model equations (13)–(14) were calculated. Then, the exactly calculated radiation supply was compared with the model output. The error of the model was normally below 2%–3%, and in extreme cases, it was below 6%. Thus, the maximum error of the new experimental setup is considerably smaller than the corresponding maximum error (about 10%–20%) of the old instrument used by Busen and Hänel (1987) as well as by Hänel et al. (1990).

In summary, the treatment of the sky radiation and the reflected radiation in the model for the radiation supply is very nearly equivalent to its measurement, with a wide-angle photometer being pointed to 48 directions in order to cover the total solid angle 4πsr.

3. Measurement of solar radiation: Instrumentation and calibration

a. Instruments

For the measurement of the components of the solar net flux density vector with respect to each of the three coordinate axes (see Table 1), we used three so-called albedometers, which are manufactured by the Adolf Thies Company. Each of these albedometers consists of two separate 2πsr pyranometers in one housing with sensors that view in opposite directions. The sky radiation was measured with a 2πsr pyranometer, manufactured by the Kipp & Zonen Company (now SCI-Tec Instruments, Inc.) in which the direct solar radiation is removed by a shadow ring. All of the instruments used in this study were protected against precipitation.

b. Mounting of instruments

To minimize mutual influences, all pyranometers are mounted at almost the same height. The arrangement of the sensors is shown in Fig. 1. In this way, the vertical components of the net flux density vector and the sky radiation are practically uninfluenced. Only the horizontal components of the net flux density vector may be somewhat biased if a minimum distance of about 1.5–2 m between neighboring instruments cannot be ensured.

c. Calibration

During the period of measurement, all pyranometers used were calibrated against an Ångström pyrheliometer. The calibration procedure was as follows. The sensors were aligned in the same way as during the measurements—that is, either horizontally or vertically. We compared two modes of measurements. First, direct solar radiation fell on the sensor, and second, it was removed shading the sensor with a disk. The difference of the pyranometer readings for these two cases was then compared with the pyrheliometer reading. For each sensor, this kind of calibration was carried out for different angles of incidence of the direct solar radiation. Thus, we obtained the calibration constant of each sensor as a function of the angle of incidence. These functions are used herein to calculate the irradiances from the pyranometer readings.

Finally, the pyrheliometer reading was compared to the World Meteorological Organization standard. Since the pyrheliometer calibration constant did not change during the last decade, we have obtained a valid calibration of all pyranometers used. The remaining errors are on the order of 1% or less.

4. Determination of the particles' mean solar volume absorption coefficient

To determine via Eq. (7) the heating rate of the atmosphere due to absorption of solar radiation by particles, the particles' mean solar volume absorption coefficient must be known. For this paper, complete sets of the optical properties of atmospheric particles, and thus also their absorption coefficient, are obtained with a method described in detail by Hänel (1994). For a short description, see Herrmann and Hänel (1997). Since the main objectives of this paper are pyranometry and parameterization of the results, we present only an outline of this method.

The atmospheric particles are sampled on Nuclepore filters, with a pore diameter of 0.2 μm. The filter is protected against precipitation, and at the same time, the sampling becomes independent of wind direction by using a special device. The volume of air sucked through the filter is measured by a gas meter.

Before and after sampling—that is, both in its unloaded and loaded state—the filter is put into a polar photometer. Therein the radiation that is transmitted plus that scattered forward by the filter and the radiation scattered backward by the filter are measured. The results of the photometric measurements are then inverted

mathematically in order to yield a complete set of the optical properties of the particles. The physical kernel of the inversion procedure is the adding method that is based on the principles of invariance—that is, an exact radiative transfer code (Hänel 1994).

The immediate results of the method are the particles' optical thickness, their single scattering albedo, and their asymmetry parameter of the phase function of scattering. Additionally, knowing the volume of air sucked through the filter and the area of the particle deposit on the filter, we obtain also the volume extinction, scattering, and absorption coefficients of the particles as mean values for the sampling period. All results are spectral mean values for extraterrestrial solar radiation from 0.3- to 3.5-μm wavelength. The results can be interpreted also as spectral values at the 0.7-μm wavelength (Blanchet 1982). Since the photometric measurements are carried out at relative humidities below 30%, the optical properties of (practically) dry particles are obtained.

Depending on the particle loading of the atmosphere, the collection of a sample of particles takes several hours at least. Consequently, using the time-averaged absorption coefficients, we may have no good resolution of the results with time. In order to improve the time resolution of the volume absorption coefficient, a method by Busen (1987) is applied. This method is based on the results from samples taken consecutively, and it presupposes that the absorption coefficient of particles varies with time according to a cubic spline. Because of this assumption, variations of the absorption coefficient during time periods that are very short, compared with the sampling time, cannot be retrieved. Thus, our result is a smoothed volume absorption coefficient versus time. (Other currently available methods allow the approximate determination of the particles' absorption coefficient via diffuse transmission measurements with a good time resolution, and thus, they have been used on flying platforms. However, in the present stage of research, the systematic errors of these methods have not been eliminated completely.)

Finally, according to Busen (1987), the absorption coefficient of dry atmospheric particles is corrected for humidity effects to obtain the particles' absorption coefficient at the observed atmospheric relative humidity. It is taken into account that the correction may be different for increasing and decreasing relative humidity.

As outlined above, the final result is the spectral mean volume absorption coefficient of atmospheric particles at ambient relative humidity versus time, which is needed to determine the heating rate according to Eq. (7).

5. Results and discussion

Normally, radiation budget measurements are restricted to the simplest atmospheric conditions: that is, clear sky, or overcast by a layer cloud. Generally, these two cases represent only extremely ideal situations, whereas situations with incomplete cloud cover are more realistic and occur frequently. Thus, we decided to make a pilot study with the aim of filling the gap between the extremes as much as possible with a limited number of measurements. Besides, we wanted to obtain and parameterize information about the variability of radiation budget properties, in particular those that are available with our novel radiation budget pyranometry.

a. Characterization of the stations and period of measurement

The measurements were taken at an urban and at a rural station. The urban station is located on the roof of the Institute of Meteorology and Geophysics in the city of Frankfurt am Main, Germany (15 m above ground, 125 m above MSL). The rural station is located about 18 km northwest of the station in the city of Frankfurt am Main on the top of Kleiner Feldberg Mountain (830 m above MSL) in the highest part of the Taunus mountain chain. Therefore, on the one hand, we have information about a polluted area with a strong influence of local, anthropogenic sources of particles and, on the other hand, we have information about a natural environment with little local, anthropogenic influence.

At the station in Frankfurt am Main, some tall buildings in the section from the east to the south shade some of the sky radiation. At the Kleiner Feldberg station the ground is covered with grass. The horizon is somewhat obstructed by laboratory containers and a small astronomical observatory in the east, as well as by trees in the south and, partially, in the north. During our measurements at both stations, the daily mean direct solar radiation was not, or was only insignificantly, reduced by the surrounding obstacles. This is of special importance for the solar radiation supply, as discussed in section 2b. The albedo at the site of the measurement was 0.12 in Frankfurt am Main and 0.17 at Kleiner Feldberg.

The optical properties of dry particles at both stations were compared directly during the period from 7 February 1996 until 12 April 1996 (Bundke 1996). During this period the mean absorption coefficient in Frankfurt am Main was about twice as high (a factor of 1.95) as that at Kleiner Feldberg. For the mean scattering coefficient, a somewhat smaller increase from the rural environment to the city (a factor of 1.76) was found. Soot was found at both stations.

Most measurements in Frankfurt am Main were taken during August and September 1997, and two were taken during December 1997. At the Kleiner Feldberg station, the measurements were taken during October and November 1997. In total, the measurements cover a period of about 5 months, from summertime to wintertime (see Table 2). Thus, we should have observed most of the variability caused by seasonal effects to be awaited in our region—for example, changes in the solar declination and in convection.

TABLE 2. Temperature, mean absorption coefficient of particles during the daylight period, maximum heating rate, and total heating during the daylight period (the integral of the heating rate during the daylight period). The heating rate and the total heating are due to absorption of solar radiation by atmospheric particles. (FFM, Frankfurt/Main; KLF, Fleiner Feldberg)

Date	Station	Temperature (°C)	Mean absorption coefficient of particles (1 km^{-1})	Maximum heating rate (K h^{-1})	Total heating during daylight period (K)
13 Aug. 1997	FFM	20°–33°	0, 0198	0, 074	0, 67
20 Aug. 1997	FFM	19°–31°	0, 0400	0, 104	0, 69
21 Aug. 1997	FFM	19°–32°	0, 0352	0, 131	1, 14
1 Sept. 1997	FFM	18°–31°	0, 0233	0, 118	0, 64
4 Sept. 1997	FFM	17°–26°	0, 0347	0, 109	0, 67
9 Sept. 1997	FFM	14°–21°	0, 0258	0, 051	0, 24
10 Sept. 1997	FFM	13°–19°	0, 0095	0, 038	0, 29
11 Sept. 1997	FFM	9°–25°	0, 0192	0, 073	0, 63
15 Sept. 1997	FFM	7°–21°	0, 0294	0, 106	0, 85
16 Sept. 1997	FFM	9°–25°	0, 0332	0, 116	1, 04
17 Sept. 1997	FFM	12°–26°	0, 0383	0, 131	0, 89
24 Sept. 1997	FFM	11°–16°	0, 0152	0, 033	0, 19
25 Sept. 1997	FFM	9°–22°	0, 0218	0, 073	0, 58
26 Sept. 1997	FFM	11°–23°	0, 0270	0, 086	0, 67
21 Oct. 1997	KLF	−2°–1°	0, 0057	0, 025	0, 13
22 Oct. 1997	KLF	0°–9°	0, 0062	0, 025	0, 18
24 Oct. 1997	KLF	0°–3°	0, 0063	0, 026	0, 08
28 Oct. 1997	KLF	−5°–−1°	0, 0047	0, 018	0, 13
29 Oct. 1997	KLF	−4°–1°	0, 0046	0, 015	0, 10
30 Oct. 1997	KLF	2°–5°	0, 0171	0, 024	0, 16
1 Nov. 1997	KLF	1°–6°	0, 0222	0, 083	0, 58
7 Nov. 1997	KLF	5°–7°	0, 0062	0, 007	0, 02
11 Nov. 1997	KLF	3°	0, 0096	0, 020	0, 03
12 Nov. 1997	KLF	2°–5°	0, 0088	0, 003	0, 02
14 Nov. 1997	KLF	2°–3°	0, 0087	0, 032	0, 11
22 Dec. 1997	FFM	2°–3°	0, 0278	0, 016	0, 03
23 Dec. 1997	FFM	3°–4°	0, 0278	0, 008	0, 03
Mean FFM			0, 0258	0, 079	0, 58
Mean KLF			0, 0091	0, 025	0, 14

b. The vector of solar net flux density

Principally, the results at both stations are similar. Therefore, we present only some exemplary cases observed at the Kleiner Feldberg station. The daily variations of the components of the vector of solar net flux density are displayed in Figs. 3a–d. The relevant sky conditions change from clear (Fig. 3a) to almost completely covered (Fig. 3d) with two intermediate stages, Figs. 3b and 3c. For details regarding the sky conditions, see the Fig. 3 caption.

On 22 October 1997 we had prevailing clear sky (Fig. 3a). The *z* component of the vector of net flux density is always negative, indicating that the vertical net flux of solar radiation is downward. Since the measurements have been taken after the equinoxes, the *y* component is always positive; that is, the net flux in the *y* direction is always from south to north. (During midsummer the *y* component becomes slightly negative shortly after sunrise and shortly before sunset.) The *x* component is negative in the morning until local noon, as direct solar radiation is incident from easterly directions, and positive later on, as the position of the sun changes from south to west. All of these main features of the clear-sky case are observed also during the cases with incomplete cloud cover, Figs. 3b and 3c. The short time variability of the vector components clearly increases if the coverage of the sky with clouds becomes larger, but it remains incomplete. If the sky is almost completely covered (Fig. 3d) both horizontal components become negligible. At the same time, the vertical component remains small.

It is of further interest that in Figs. 3a–c the maximum absolute value of the *z* component is considerably smaller than the values of the other components. This is due to the low position of the sun during October.

The results in Fig. 3a suggest that the optimal period for the absorption determination via the simplified divergence measurement [according to the approximation made in Eq. (6)] is a small time interval around local noon. Then, the *x* component of the net flux density vector changes rapidly with time but remains negligible, and the *y* and *z* components remain almost constant. According to Busen and Hänel (1987), Hänel et al. (1990), and Fig. 4b, this is the time period during clear-sky conditions when the absorption of solar radiation is maximum or almost maximum. However, during incomplete cloudiness, the maximum absorption must not be found around local noon, and can be more than twice as large as the mean absorption during the daylight period [Hänel et al. (1990) and Fig. 4b]. The mean absorption is the property that is more relevant to climate.

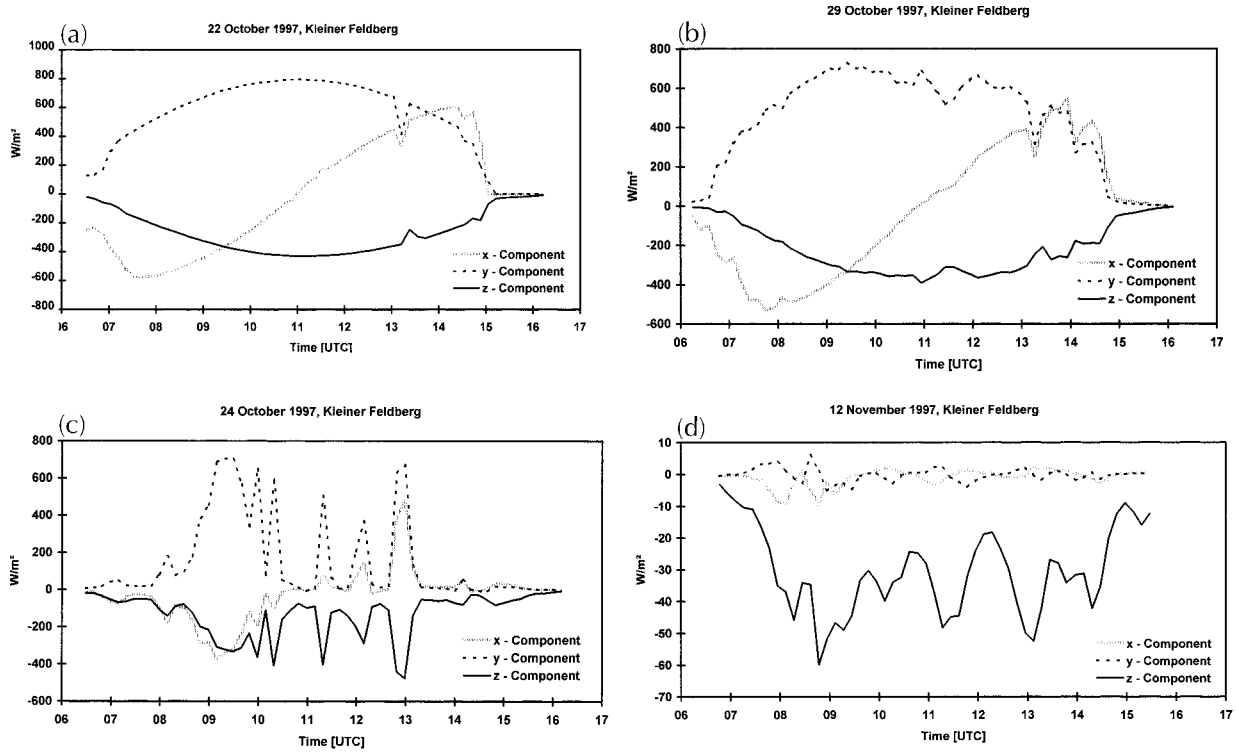

FIG. 3. Components of the vector of solar net flux density at the Kleiner Feldberg station. Results for different sky conditions. (a) 22 October 1997. Mostly clear. In the afternoon there are a few cirrus clouds. The total cloud coverage ranges from 0 to 1/8. (b) 29 October 1997. Partly clear. Partly cirrostratus, cirrocumulus, altostratus, and altocumulus clouds are present. The total cloud coverage ranges from 2/8 to 6/8. (c) 24 October 1997. Broken cloudiness with some gaps. Cumulus humilis, stratocumulus, and cirrus clouds. The total cloud coverage ranges from 4/8 to 7/8. (d) 12 November 1997. Almost completely covered with stratocumulus and stratus clouds. The total cloud coverage ranges from 7/8 to 8/8.

c. Solar radiation supply

The radiation supply is the integral of the radiance over all directions [Eq. (3)]. Since the radiance itself, instead of its components, is integrated and the integration takes place over all directions, the radiation supply becomes considerably larger than the direct solar radiation or the global radiation. Especially during summertime and scattered cloudiness, the radiation supply value may reach or considerably exceed that of the solar constant [see, e.g., Busen and Hänel (1987) and Fig. 4a].

As shown in Fig. 4a, the daily mean solar radiation supply at the Kleiner Feldberg station decreases with increasing cloudiness. However, the largest value of the solar radiation supply in Fig. 4 does not occur during the clear-sky case (22 October 1997) but during a day with moderate-to-strong cloudiness and with cumulus clouds present (24 October 1997). In such a case, we may observe direct solar radiation, as well as intensive radiation from the sides of nearby cumulus clouds. This leads to large, transient spikes of the solar radiation supply, as has been observed repeatedly.

Corresponding results as for the radiation supply have been reported also for the global radiation (Duchon and O'Malley 1999) and the part of the actinic flux in the UV-B (which is the radiation supply in the UV-B) arising from downwelling radiation (A. Rüb 1999, personal communication). The latter has been measured for about one year at the Kleiner Feldberg station.

For simple estimates of the atmospheric heating by absorption of solar radiation, a parameterization of the solar radiation supply is needed. Since the flux density of direct solar radiation and the global radiation are easily accessible, either by measurements or by parameterizations (e.g., see Iqbal 1983), we studied the validity of a simple approximation equation by Busen and Hänel 1987). This equation is based on the assumption that both the sky radiation and the reflected radiation are isotropic. It reads

$$S = F_S + 2H_{-Z,\mathrm{SKY}} + 2H_Z = (1 - 2|\cos\theta_S|)F_S + 2(1 + \alpha)H_{-Z}, \quad (16a)$$

where α is the albedo. In this formula, we split the global radiation into its direct and diffuse part

$$H_{-Z} = |\cos\theta_S|F_S + H_{-Z,\mathrm{SKY}} \quad (16b)$$

and yielded

$$S = (1 + 2\alpha|\cos\theta_S|)F_S + 2(1 + \alpha)H_{-Z,\mathrm{SKY}}. \quad (16c)$$

For the sky radiation as function of the cloud cover, we used the relationship

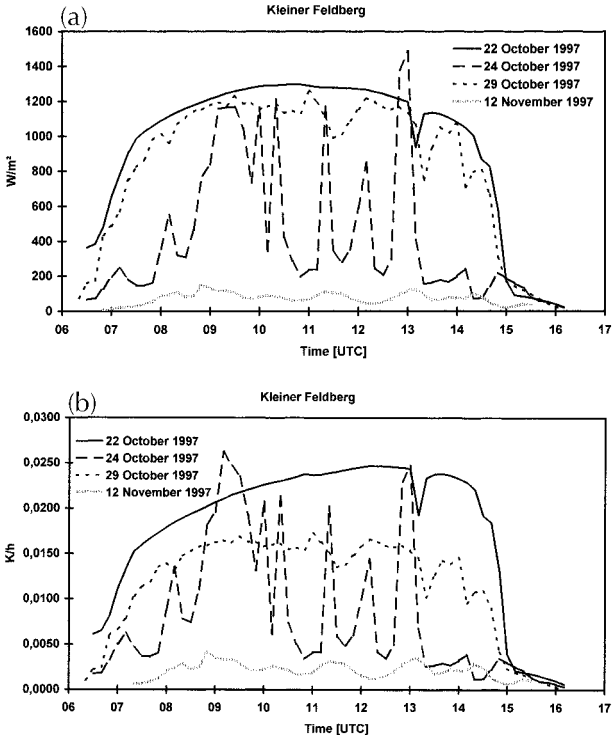

FIG. 4. (a) Solar radiation supply and (b) heating rate of the air due to absorption of solar radiation by atmospheric particles at the Kleiner Feldberg station at different sky conditions. The results from the same days as in Fig. 3 are displayed.

$$H_{-Z,\mathrm{SKY}} = h_0 + h_1 c + h_2 c^2 + h_3 c^3, \tag{16d}$$

where c is the dimensionless cloud cover varying from 0 to 1. The constants in Eq. (16d), all in watts per square meter, have been deduced from our measurements and are $h_0 = 98.83$, $h_1 = -474.25$, $h_2 = 1645.2$, and $h_3 = -1155.1$ for Frankfurt am Main, and $h_0 = 37.96$, $h_1 = -76.93$, $h_2 = 634.5$, and $h_3 = -560.7$ for Kleiner Feldberg. Normally, the diffuse radiation should be parameterized also as a function of cloud type (e.g., Burridge and Gatt 1974). However, because of a lack of sufficient data, this could not be performed in this study.

In order to compare the parameterized and measured solar radiation supply, we used the direct solar radiation as measured, and we used the diffuse-sky radiation as approximated by Eq. (16d). In Fig. 5, a good overall agreement between parameterized and measured solar radiation supply is shown. According to our procedure, the scattering of the data points results only from the use of approximation Eq. (16d) for the diffuse-sky radiation. Consequently, we conclude that in estimating the radiation supply it is very important to know as precisely as possible the direct solar radiation, because if direct solar radiation is present and the sun is not too close to the horizon, the radiation supply consists mostly of direct radiation.

Finally, it is important to obtain some insight into the influence of the albedo on the radiation supply. For this

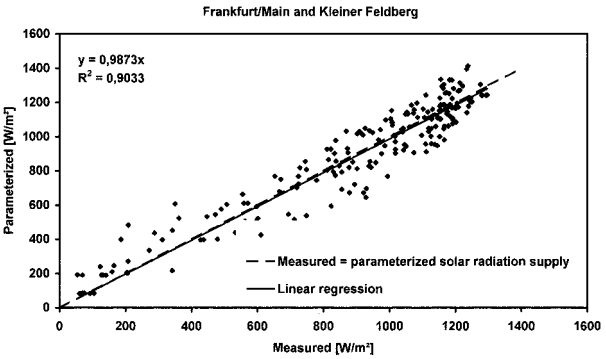

FIG. 5. Parameterized vs measured solar radiation supply. All results from measurements taken at Frankfurt am Main and Kleiner Feldberg are incorporated.

a parameterization of sky radiation in Eq. (16a) or (16c) as a function of the albedo is needed. The relevant equation is derived converting the vector equation for the sky radiation from the adding method [see Hänel 1994, third equation in (A1)] into a scalar form. It reads

$$H_{-Z,\mathrm{SKY}} = [H_{-Z,\mathrm{SKY}}(\alpha = 0) + \alpha b_{\mathrm{ATM}} |\cos\theta_S| F_S] \div (1 - \alpha b_{\mathrm{ATM}}), \tag{17a}$$

where b_{ATM} is the fraction of radiation scattered by the atmosphere to the ground when illuminated from below, and where $1/(1 - \alpha b_{\mathrm{ATM}})$ is the enhancement factor due to multiple radiative interactions between the atmosphere and the ground. Introducing Eq. (17a) into (16c) and differentiating the result with respect to the albedo α yields

$$\frac{dS}{d\alpha} = 2\frac{1 + b_{\mathrm{ATM}}}{(1 - \alpha b_{\mathrm{ATM}})^2}[|\cos\theta_S| F_S + H_{-Z,\mathrm{SKY}}(\alpha = 0)]. \tag{17b}$$

Since $H_{-Z,\mathrm{SKY}}(\alpha = 0) \le H_{-Z,\mathrm{SKY}}$, it follows from (16b) that $H_{-Z}(\alpha = 0) \le H_{-Z}$ and

$$\frac{dS}{d\alpha} \le 2\frac{1 + b_{\mathrm{ATM}}}{(1 - \alpha b_{\mathrm{ATM}})^2} H_{-Z}. \tag{17c}$$

From Eqs. (17b) and (17c) it can be seen that the change of the radiation supply with the albedo is large, when both the albedo and the backscattering by the atmosphere are large. This is the case when at the same time the ground is covered with fresh snow and the sky is completely covered by a highly backscattering cloud layer. Please note that an average albedo for the area surrounding the station (about a 20-km distance or more)—not the local albedo at the site of the measurement—must be introduced into the formulas (17a), (17b), and (17c).

Since during our measurements the ground was not covered with snow, the average albedos of the areas around the stations were estimated (considering land use) to range between 0.15 and 0.20. The sky ranged from very clear ($b_{\mathrm{ATM}} <$ about 0.1) to almost completely

covered with clouds ($b_{ATM} <$ about 0.5–0.7). Thus, we are able to estimate from Eq. (17c) $dS/d\alpha < 2.3H_{-Z}$ to $4.6H_{-Z}$. Finally, the uncertainty $\Delta\alpha = 0.05$ of the mean albedos estimated above for the stations can be introduced into Eq. (17d). This yields the maximum uncertainty of the radiation supply at both stations, as caused by the uncertainty of the albedo estimates to be smaller than 11%–23% of the global radiation. Consequently, regarding the situations during our measurements, a difference of the mean albedo among both stations cannot be expected to cause an extreme difference of the radiation supply. The same holds via Eq. (7), also for the heating rates at both stations.

d. Heating rate and total heating during the daylight period

The heating rates of the atmosphere due to absorption of solar radiation by atmospheric particles are shown in Fig. 4b for the same days as in Fig. 4a. The heating rate is proportional to the product of the particles' mean solar volume absorption coefficient and the solar radiation supply [Eq. (7)]. Therefore, the heating rates in Fig. 4b have features similar to those of the solar radiation supply in Fig. 4a. However, the details and relative levels of corresponding curves differ. This is caused by the influence of the particles' mean solar volume absorption coefficient—that is, the local absorber level—on the heating rate.

All of our experimental results of the maximum heating rate and the total heating during the entire daylight period are compiled in Table 2. The results show that the maximum heating rate varied in Frankfurt am Main between 0.008 and 0.131 K h^{-1}—that is, by a factor of about 17. The variation at Kleiner Feldberg was between 0.003 and 0.083 K h^{-1}—that is, by a factor of about 28. The mean particle's absorption coefficient during the daylight period (Table 2) varied in Frankfurt am Main by a factor of 4.0, and at Kleiner Feldberg by a factor of 4.8. Thus, at both stations, the variability of the maximum heating rate is caused by the variabilites of both the particles' absorption coefficient and the radiation supply. In the mean, the maximum heating rate in Frankfurt am Main is about three times larger than at Kleiner Feldberg. This is caused mainly by the much larger absorption coefficients of the particles in Frankfurt am Main compared with those at Kleiner Feldberg (Table 2). This difference should be due mostly to the local anthropogenic sources of soot in Frankfurt am Main. Soot is regarded to be the main absorber of solar radiation.

The total heating during the daylight period varies between 0.03 and 1.14 K—a factor of 38—in Frankfurt am Main, and between 0.02 and 0.58 K—a factor of 29—at Kleiner Feldberg. In Frankfurt am Main the mean value is more than four times larger than it is at Kleiner Feldberg.

The daily mean irradiance at the top of the atmosphere undergoes a seasonal change, with a maximum during the summer solstice and a minimum during the winter solstice. Consequently, via the radiation supply, the maximum heating rate and the total heating during the daylight period should undergo a seasonal change, too. On the other hand, the variabilities of the cloud cover and cloud type, as well as the variabilities of the particles' absorption coefficient, should mask this change. The values of the maximum heating rate and the total heating during the daylight period are in accordance with these expectations, as shown in Table 2.

A further astonishing and important result of our measurements is that the values for the maximum heating rate and the total heating during the daylight period correspond very well. To obtain a relationship between both properties, all clear- and cloudy-sky cases from both stations (see Table 2) have been used. A linear regression yields

$$\Delta T = 7.88\left(\frac{dT}{dt}\right)_{\max} - 0.05 \text{ K}, \qquad (18)$$

where ΔT is the total heating during the daylight period. The coefficient of determination equals 0.93. Equation (18) together with Eq. (7) as well as Eq. (16a) or (16c), allow simple estimates of the total heating during the daylight period for any absorbers whose absorption coefficients are known. For absorption coefficients of wet and dry particles and water vapor, see, for example, Busen and Hänel (1987), Hänel et al. (1990), and Hänel (1987). Humidity correction factors for the particles' absorption coefficient are given by Hänel et al. (1990). In the present stage of research, Eq. (18) holds only for Frankfurt am Main and Kleiner Feldberg. Further studies at other locations will be necessary to prove whether or not Eq. (18) can be applied more generally.

e. Comparison of results from the last four decades

The total heating of the atmosphere during the daylight period due to absorption of solar radiation by atmospheric particles is of importance regarding the atmospheric radiation budget and thereby long-term weather and climate prediction. For a discussion of this, in Table 3, we have compiled the variability of the heating in the lowest kilometer of the atmosphere [because of the regression equation (18)] as well as the variability of the maximum heating rate. In total, the results from 105 days of observations during the last four decades from different regions of the Northern Hemisphere are displayed. The main findings are the following:

1) The maximum heating rate varies between 0.008 and 0.36 K h^{-1} (a factor of 45).
2) The total heating during the daylight period varies between 0.02 and 1.43 K (a factor of 72)—that is, almost twice as much.
3) Virtually the same variabilities have been found during the four decades in which all of the regions have

TABLE 3. Variabilities from this study and others of the maximum heating rate and the total heating during the daylight period in the lowest kilometer of the atmosphere. The following are the location abbreviations. ECH: English Channel; FFM: Frankfurt am Main, city, 125 m above MSL (Germany); KLF: Kleiner Feldberg, Taunus Mountains nearby FFM, 830 m above MSL (Germany); MTO: Monteombraro, Appennines, nearby PIU, 720 m above MSL (northern Italy), PIU: Piumazzo, Po Valley, 64 m above MSL (northern Italy); TOK: Tokyo (Japan).

Author	Location, number of days	Time	Maximum heating rate (K h^{-1})	Total heating during daylight period (K)
Roach (1961)	ECH, 9	April–October 1959	0.025–0.13* 0.012–0.25**	
Murai et al. (1976)	TOK, 5	November 1974–January 1975	0.013–0.13	
Busen (1987)	PIU and MTO, 15	October 1985	0.013–0.36	0.08–1.43
Busen and Hänel (1987)	FFM, 29	January 1982–February 1984	0.029–0.28	0.05–1.26
Hänel et al. (1990)	FFM, 7	January and March 1987	0.012–0.26	0.06–1.32
Hannesen (1995)	FFM and KLF, 13	January–May 1995	0.014–0.14	0.08–0.56
This study	FFM and KLF, 27	August–December 1997	0.008–0.13	0.02–1.14

* Mean values for the lowest 10 000 ft of the atmosphere.
** Layer adjacent to the surface.

been studied. Consequently, the observed variability of the absorption of solar radiation by particles is a long-term and widespread phenomenon in the Northern Hemisphere.

The total heating during the daylight period by absorption of solar radiation within particles is a measure of the radiative forcing by absorbing particles in the atmospheric boundary layer. Its values range from negligible to considerable forcing. Since even small radiative forcings of the atmosphere may become important when integrated over sufficiently long periods of time, the absorption of solar radiation by particles should be taken into account regarding climate forecast and perhaps also weather forecast for periods longer than one to two weeks. In this sense, parameterizations like those presented in this paper should help to eliminate the present uncertainties regarding the total heating of the planetary boundary layer during the daylight period.

6. Conclusions

Our measurements show the following features: 1) In cloudy-sky conditions, the solar radiation supply at the ground may reach or surpass the solar constant—that is, about 1300–1400 W m^{-2}. 2) There is no daytime period during which all of the components of the vector of net flux density remain constant. The optimum period for the simplified net flux divergence measurements commonly undertaken is a short time interval around local noon. 3) The solar radiation supply, the solar net flux density vector, and the atmospheric heating rate undergo extreme variations with time when scattered clouds are present. 4) The solar radiation supply can be calculated simply and accurately when the flux densities of the direct solar radiation and the global or the diffuse radiation are known. 5) There is an approximately linear relationship between the maximum heating rate of the atmosphere due to absorption of solar radiation by particles and the appertaining total heating during the entire daylight period that holds for all sky conditions and seasons. 6) Finally, it is shown that the same variabilities of the maximum heating rate and the total heating have been measured for decades by various authors in different parts of the Northern Hemisphere. The total heating during the entire daylight period varies between 0.02 K (negligible radiative forcing) and 1.4 K (significant radiative forcing of the atmospheric boundary layer).

REFERENCES

Ambach, W., 1963: Untersuchungen zum Energieumsatz in der Ablationszone des grönländischen Inlandeises. *Meddelser om Grønland*, **174,** 1–206.

Blanchet, J.-P., 1982: Application of the Chandrasekhar mean to aerosol optical parameters. *Atmos.–Ocean*, **20,** 189–206.

Bundke, U., 1997: Optische Eigenschaften atmosphärischer Teilchen: Teilchen im Stadtgebiet von Frankfurt am Main und Vergleich zwischen Frankfurt und dem Kleinen Feldberg (Taunus). Diploma thesis, Institute of Meteorology and Geophysics, Johann Wolfgang Goethe University, 182 pp. [Available from Institute of Meteorology and Geophysics, Johann Wolfgang Goethe University, Georg Voigt Strasse 14, D-60325 Frankfurt am Main, Germany.]

Burridge, D. M., and A. J. Gadd, 1974: The Meteorological Office operational 10 level numerical weather prediction model (December 1974). The Met. Office Tech. Notes 12 and 48, 57 pp. [Available from The Met. Office, London Rd., Bracknell, Berkshire, RG12 2SZ United Kingdom.]

Busen, R., 1987: Die Absorption solarer Strahlung in der Atmosphäre: Meßtechnik und meteorologische Auswertung. Ph.D. thesis, Johann Wolfgang Goethe University, Frankfurt am Main, Germany.

——, and G. Hänel, 1987: Radiation budget of the boundary layer. Part I: Measurement of absorption of solar radiation by atmospheric particles and water vapor. *Contrib. Atmos. Phys.*, **60,** 229–240.

Duchon, C. E., and M. S. O'Malley, 1999: Estimating cloud type from pyranometer observations. *J. Appl. Meteor.*, **38,** 132–141.

Hänel, G., 1987: Radiation budget of the boundary layer. Part III: The mean solar volume absorption coefficients of water vapor for direct and diffuse radiation. *Contrib. Atmos. Phys.*, **60,** 248–254.

——, 1994: Optical properties of atmospheric particles: Complete parameter sets obtained through polar photometry and an improved inversion technique. *Appl. Opt.*, **33,** 7187–7199.

——, R. Busen, C. Hillenbrand, and R. Schloss, 1982: Light ab-

sorption measurements: New techniques. *Appl. Opt.,* **21,** 382–386.

——, D. Weidert, and R. Busen, 1990: Absorption of solar radiation in an urban atmosphere. *Atmos. Environ.,* **24B,** 283–292.

Hannesen, R., 1995: Die Erwärmungsrate der Atmosphäre durch Absorption solarer Strahlung in Aerosolpartikeln. Diploma thesis, Johann Wolfgang Goethe University, Frankfurt am Main, Germany.

Herrmann, P., and G. Hänel, 1997: Wintertime optical properties of atmospheric particles and weather. *Atmos. Environ.,* **31,** 4053–4062.

Iqbal, M., 1983: *An Introduction to Solar Radiation.* Academic Press, 390 pp.

Murai, K., M. Kobayashi, R. Goto, and T. Yamuachi, 1976: The absorption of solar radiation in the lower atmosphere. *Pap. Meteor. Geophys.,* **27,** 21–32.

Roach, W. T., 1961: Some aircraft observations of fluxes of solar radiation in the atmosphere. *Quart. J. Roy. Meteor. Soc.,* **87,** 346–363.

Valero, P. J., W. J. Y. Gore, and L. P. M. Giver, 1982: Radiative flux measurements in the troposphere. *Appl. Opt.,* **21,** 831–838.